



1 **Solar occultation measurement of mesospheric ozone by**  
2 **SAGE III/ISS: Impact of variations along the line of sight**  
3 **caused by photochemistry**

4

5 **Murali Natarajan <sup>1</sup>, Robert Damadeo <sup>1</sup>, David Flittner <sup>1</sup>**

6 <sup>1</sup> Science Directorate, NASA Langley Research Center, 21 Langley Blvd., Mail Stop 401-B,  
7 Hampton, VA 23681, USA.

8 Correspondence to: Murali Natarajan ([murali.natarajan@nasa.gov](mailto:murali.natarajan@nasa.gov))

9

10 **Abstract.** Twilight gradients in the concentration of atmospheric species with short  
11 photochemical lifetimes influence the transmission data obtained in a solar occultation  
12 instrument like the Stratospheric Aerosol and Gas Experiment III aboard the International Space  
13 Station (SAGE III/ISS). These photochemically induced changes result in nonlinear asymmetries  
14 in the species distribution near the tangent altitude along the line of sight (LOS). The bias  
15 introduced by neglecting the effects of twilight variations in the retrieval of mesospheric ozone is  
16 the focus of this study. O<sub>3</sub> in the mesosphere exhibits large variations near the terminator during  
17 sunrise and sunset based on current understanding of the photochemistry of this altitude region.  
18 The algorithm used in the SAGE III/ISS standard retrieval procedure for mesospheric ozone does  
19 not include the effects of these gradients. This study illustrates a method for implementing a  
20 correction scheme to account for the twilight variations in mesospheric O<sub>3</sub> and gives an estimate  
21 of the error in the standard retrieval. We use the results from a diurnal photochemical model



22 conducted at different altitudes to develop a database of ratios of mesospheric O<sub>3</sub> at different  
23 zenith angles around 90° to O<sub>3</sub> at a zenith angle of 90° for both sunrise and sunset conditions.  
24 These ratios are used to scale the O<sub>3</sub> at levels above the tangent altitude for appropriate zenith  
25 angles in the calculation of the optical depth along the LOS. In general, the impact of the twilight  
26 variations is to increase the optical depth thereby reducing the retrieved O<sub>3</sub> concentration at the  
27 tangent altitude. We find that at sunrise the mesospheric O<sub>3</sub> including the diurnal corrections is  
28 lower by more than 20% compared to the archived O<sub>3</sub>. We show the results obtained for different  
29 latitudes and seasons. In addition, for nearly co-located sunrise and sunset scans, we note that  
30 these corrections lead to better qualitative agreement in the sunrise to sunset O<sub>3</sub> ratio with the  
31 photochemical model prediction.

32

### 33 **1 Introduction**

34

35 The solar occultation measurement technique has been the workhorse among various methods  
36 used for monitoring the composition of the earth's atmosphere for over 4 decades. This is  
37 evidenced by many successful experiments such as SAGE, SAGE II, HALOE, ATMOS, ACE-  
38 FTS, POAM, SAGE III/M3M and SAGE III/ISS. Major advantages of this technique include  
39 high signal to noise ratio, high vertical resolution, longer path length, and long-term accuracy  
40 provided by the 'self-calibrating' nature of the instrument operation. Limited global coverage  
41 ranks high among the disadvantages of this method. In the occultation experiments, the  
42 absorption of solar radiance measured by the instrument as a function of tangent height altitude  
43 or pressure is related to the optical depth and hence the abundance of the species along the line of  
44 sight (LOS). The bulk of the absorption, in general, occurs around the tangent point because of



45 the exponential decrease in atmospheric density with altitude and due to the slant path  
46 determined by the spherical geometry. Standard algorithms used in the retrievals assume that the  
47 species distribution in atmospheric layers is homogeneous and, therefore, the distribution along  
48 the LOS is symmetrical around the tangent point location. This assumption is quite valid for  
49 species such as CH<sub>4</sub>, H<sub>2</sub>O, and stratospheric O<sub>3</sub> because of their long photochemical lifetimes. In  
50 the case of species with short lifetimes, the sudden changes in the photolysis rates near day/night  
51 terminator trigger rapid variations in the concentration as a function of zenith angle. These  
52 variations result in nonlinear asymmetry along the LOS.

53

54 The influence of twilight variations in NO and ClO on the interpretation of solar occultation  
55 measurements was described by Boughner et al. (1980). Correction factors based on  
56 photochemical models, as discussed in the above study, have been routinely applied in the  
57 retrievals of stratospheric NO and NO<sub>2</sub> profiles in HALOE (Gordley et al., 1996; Russell et al.,  
58 1988) and in ATMOS (Newchurch et al., 1996). Brohede et al. (2007) described the role of  
59 diurnal variations in the retrieval of NO<sub>2</sub> from OSIRIS measurements. The algorithm used in the  
60 retrieval of NO<sub>2</sub> in SAGE, SAGE II, SAGE III/M3M, and SAGE III/ISS neglects the twilight  
61 variations. Recent study of the NO<sub>2</sub> retrieval from SAGE III/ISS by Dube et al. (2021) describes  
62 the importance of considering the diurnal variations along the LOS.

63

64 Mesospheric O<sub>3</sub> is also characterized by short photochemical lifetimes and steep twilight  
65 gradients and, therefore, it is a potential candidate species requiring appropriate corrections in a  
66 retrieval from solar occultation instruments. Natarajan et al. (2005) noted that the diurnal  
67 correction factors used in the retrieval of mesospheric ozone from HALOE (Version 19) needed



68 to be updated. The new factors were derived from a diurnal photochemical model of mesospheric  
69 ozone. They illustrated the impact of the corrections using a small subset of retrieved HALOE  
70 mesospheric O<sub>3</sub> profiles. In the present study, we describe the application of similar corrections  
71 to the SAGE III/ISS retrieval of mesospheric O<sub>3</sub>. Table 1 of the Data Product User's Guide for  
72 SAGE III/ISS (2021) lists the release status of mesospheric O<sub>3</sub> data as a Beta version that is yet  
73 to be validated, because it is still potentially impacted by spectral stray light within the  
74 instrument. Our goal is to quantify the impact of the corrections on the archived data and to see  
75 whether the changes can support other known criteria. A description of the mesospheric O<sub>3</sub>  
76 variations under twilight conditions as calculated with a diurnal photochemical model is given in  
77 section 2. The occultation geometry and the diurnal correction factors for mesospheric O<sub>3</sub> are  
78 described in section 3. Results from the application of the factors to correct the archived data are  
79 discussed in section 4. We also include the results from an approximate retrieval using the  
80 archived transmission data with and without diurnal corrections. This is followed by a discussion  
81 of sunrise to sunset mesospheric O<sub>3</sub> ratios using appropriate co-located scans and a comparison  
82 to theoretical values. The final summary section reiterates the importance of corrections for  
83 photochemically induced twilight mesospheric O<sub>3</sub> variations in solar occultation retrievals.

84

## 85 **2 Mesospheric O<sub>3</sub> variations at sunrise/sunset**

86

87 Diurnal variations in reactive species can be obtained using a time-dependent diurnal  
88 photochemical model. A detailed description of the model used in this study is given in  
89 Natarajan et al. (2005). For the present study, we have updated the chemical rate constant data  
90 using the JPL Publication 19-5 (2020). Calculated diurnal O<sub>3</sub> variation in June at the latitude of



91 11.25°S and at different altitudes of interest to this work is illustrated in Figure 1. O<sub>3</sub>  
92 concentration is shown as a function of time starting at midnight. Nighttime O<sub>3</sub> has a constant  
93 value representing the total odd oxygen in the lower mesosphere. A sharp decrease at sunrise is  
94 mainly caused by photolysis of O<sub>3</sub> forming atomic oxygen. The recombination of atomic oxygen  
95 and O<sub>2</sub> quickly balances the loss of O<sub>3</sub> from photolysis. This reaction is pressure dependent and  
96 becomes slower at higher altitudes. The photolysis of O<sub>2</sub> generates additional odd oxygen (O<sub>X</sub> =  
97 O + O<sub>3</sub>) and in the morning hours this leads to an increase in both O<sub>X</sub> and O<sub>3</sub>. The formation of  
98 odd hydrogen species from the reaction of O(1D) with H<sub>2</sub>O during the day triggers the catalytic  
99 destruction of odd oxygen through reactions involving OH. It is noted that in this altitude range  
100 odd oxygen itself has a daytime variation caused by the competing production and destruction  
101 reactions. In the early morning there is a net gain of O<sub>X</sub> and in the evening there is net loss of  
102 O<sub>X</sub>, which continues even after sunset until atomic oxygen is depleted. The large increase in O<sub>3</sub>  
103 seen after sunset is mainly due to the recombination of atomic oxygen and O<sub>2</sub>. At higher  
104 altitudes, not shown here, model predictions indicate a dramatic shift in the diurnal behavior of  
105 O<sub>3</sub>. The diurnal model extends to 100 km; however, since the quoted uncertainty above 70 km in  
106 the archived SAGE III/ISS O<sub>3</sub> is large, we will focus on the region below 70 km.

107

108 The results of the full diurnal cycle are of general interest about the model simulation. But, with  
109 reference to solar occultation measurements, the sharp gradients seen in the O<sub>3</sub> concentration  
110 near a zenith angle of 90° are more critical. The significance of the twilight variations to the  
111 retrieval of mesospheric O<sub>3</sub> under sunrise/sunset conditions can be understood with the help of  
112 the schematic shown in Figure 2. This illustrates the occultation geometry in the plane containing  
113 the LOS. The red line denotes the LOS at a tangent altitude of Z<sub>T</sub>. Points F and N represent the



114 intersection of the LOS with an atmospheric layer at an altitude of  $Z$  shown in green. For a  
115 species with little or no twilight variations, the concentrations at the locations F and N are nearly  
116 equal to that at the location U, the tangent point at an altitude of  $Z$ . In this case, the  
117 concentrations at tangent height  $Z_T$  can be derived in a straightforward manner from the  
118 measured transmission using a retrieval algorithm. However, if the photochemistry causes  
119 significant gradients near  $90^\circ$ , as in the case of mesospheric  $O_3$ , the distribution around the  
120 tangent point becomes nonlinearly asymmetric because the concentrations at F and N depend on  
121 the respective local zenith angles. This variation must be incorporated in the evaluation of  $O_3$   
122 specific optical depth along the LOS.

123

124 To illustrate the impact of diurnal variations on slant-path column of  $O_3$ , we selected a typical  
125 event from the SAGE III/ISS data and applied the calculated  $O_3$  variations in the slant-path  
126 column evaluation. The required parameters include month, date, event type (sunrise or sunset),  
127 tangent altitude, latitude, longitude, spacecraft latitude and longitude. These data are taken from  
128 the current Version 5.2 SAGE III/ISS data available from the Atmospheric Sciences Data Center  
129 (ASDC) at NASA LaRC. We used the model results for June at  $11.25^\circ\text{S}$  latitude to get the  $O_3$  at  
130 sunrise variation along the LOS corresponding to different tangent altitudes from 56 to 76 km.  
131 The latitude of the chosen SAGE III/ISS measurement is  $11.35^\circ\text{S}$ . The results for tangent altitude  
132 of 64 km are shown in the left panel of Figure 3. The X-axis shows the distance along the LOS  
133 relative to the tangent point with positive direction towards instrument and negative direction  
134 towards the Sun. Corresponding zenith angles are shown at the top. The dotted line corresponds  
135 to the  $O_3$  concentration along the LOS when the diurnal variations are neglected and only the  
136 values corresponding to  $90^\circ$  zenith angle from the layers above the tangent altitude are used. The



137 solid line represents the  $O_3$  including the diurnal variations at the respective altitudes. The  
138 increased  $O_3$  concentrations on the instrument side of the LOS is readily seen. The ratio of the  $O_3$   
139 column along the LOS with diurnal variations to the column without the diurnal variations is  
140 shown as a function of tangent altitude in the panel on the right side. The peak difference of the  
141 order of 30% occurs in the altitude range from 61 to 72 km. Underestimation of the  $O_3$  slant-path  
142 column in the standard retrieval translates to overestimation of the retrieved  $O_3$ . The error  
143 committed by the neglect of twilight variations can be evaluated with the help of the diurnal  
144 model results.

145

146 The technique is to express the  $O_3$  variation as a function of zenith angle in terms of  
147 concentration normalized to  $O_3$  at a zenith angle of  $90^\circ$ . Figure 4 shows the distribution of the  
148 ratio  $O_3/O_3(\theta=90^\circ)$  near sunrise as a function of zenith angle and altitude obtained from the  
149 model results for  $11.25^\circ\text{S}$  latitude in June. For a given tangent height, the total slant-path  $O_3$   
150 column comprises of partial slant-path columns corresponding to the layers at and above the  
151 tangent height. Spherical geometry dictates that the partial pathlength along the LOS is  
152 maximum for the layer immediately above the tangent height (i.e., the lowest layer) and  
153 decreases dramatically for higher layers. This, combined with decreasing  $O_3$  concentration with  
154 height in the lower mesosphere, results in a total slant-path column dominated by contributions  
155 from a few layers right above the tangent point. Therefore, only a small range of zenith angles,  
156 say between  $86^\circ$  and  $94^\circ$ , centered at  $90^\circ$  are important. At 62 km the  $O_3$  ratio is less than 1.0 for  
157 zenith angle less than  $90^\circ$  and it increases gradually for zenith angles greater than  $90^\circ$ . At higher  
158 altitudes, the ratio shows a much steeper increase for zenith angles greater than  $92^\circ$ . The ratio, in



159 some cases, is even slightly larger than 1.0 at zenith angles less than  $90^\circ$ . From the occultation  
160 geometry shown in Figure 2, it is seen that as one moves away from a zenith angle of  $90^\circ$  along  
161 the LOS at any tangent altitude, the corresponding altitude layer of interest moves upwards.  
162 Figure 5 illustrates the  $O_3$  twilight ratio as a function of zenith angle and altitude for sunset  
163 conditions for the same latitude and month. The changes in the ratio for sunset condition are  
164 smaller and more gradual especially for zenith angles greater than  $90^\circ$  compared to the sunrise  
165 case. It should be recalled that the daytime variation in the odd oxygen concentration in the  
166 lower mesosphere impacts the  $O_3$  concentration differently at sunrise and sunset. The differences  
167 between the  $O_3$  variations for sunrise and sunset conditions suggest that the effects on the  
168 retrievals are different for sunrise and sunset occultations. The twilight  $O_3$  ratios for altitude  
169 layers above the tangent altitude can be used to get the  $O_3$  concentration and hence the optical  
170 depth along the LOS more accurately. An earlier study with HALOE mesospheric  $O_3$  data  
171 (Natarajan et al. 2005), showed that the twilight ratio is quite robust and small changes in the  
172 atmospheric parameters such as temperature and  $H_2O$  do not impact this ratio much.

173

### 174 **3 SAGE III/ISS Mesospheric ozone**

175

176 The Sage III/ISS instrument payload was launched in February 2017 and successfully attached to  
177 the ISS. The ISS occupies a low earth orbit at an inclination of  $51.64^\circ$  that provides occultation  
178 coverage of low- and mid-latitude regions. Description of the experiment and early validation of  
179 the  $O_3$  measurements are given in McCormick et al. (2020) and Wang et al. (2020). More  
180 detailed information on the various wavelength channels and data used for retrieving a suite of  
181 atmospheric species including mesospheric  $O_3$  are given in SAGE III Algorithm Theoretical



182 Basis Document (ATBD, 2002) and in the SAGE III/ISS Data Products User's Guide Version  
183 3.0 (2021) (DPUG). Among the three different O<sub>3</sub> profile measurements made by the instrument,  
184 the one based on short wavelengths in the Hartley-Huggins bands refers exclusively to  
185 mesospheric O<sub>3</sub>. Three Charge-Coupled Device (CCD) pixel groups (PGs 0-2) are assigned to  
186 the short wavelengths in the 280 – 293 nm range, though only one (PG 1 centered at 286 nm) is  
187 currently used for the retrieval. According to the DPUG, mesospheric O<sub>3</sub> data have not been  
188 fully validated. We also note that the uncertainty in the archived O<sub>3</sub> concentration becomes  
189 larger than 10% above 70 km and there are some spurious negative data pointing to uncertainties  
190 in the transmission. The present study focusses only on SAGE III/ISS O<sub>3</sub> in the lower  
191 mesosphere up to an altitude of 70 km even though the retrieval itself starts at 90 km. The  
192 diurnal model described in the previous section extends up to 100km. We use the Version 5.2  
193 transmission and species data obtained from ASDC at NASA LaRC. For each year and month,  
194 we have categorized the scans according to event type, sunrise, or sunset. The input data for our  
195 analysis include the tangent point latitude and longitude, spacecraft latitude and longitude,  
196 vertical profiles of neutral density, mesospheric O<sub>3</sub>, and transmission. We use only the  
197 transmission data from the science pixel group 1 (PG1), which has a center wavelength of  
198 286.124 nm, since the predominant species active in this wavelength region is O<sub>3</sub>.  
199

200 A database of O<sub>3</sub> twilight ratios for sunrise and sunset conditions has been generated from the  
201 diurnal model results. These ratios cover for each month the latitude range from 56.25°N to  
202 56.25°S at an interval of 11.25°, zenith angles from 84° to 96° at 0.5° intervals, and altitudes  
203 from 56 to 90 km at 0.5 km intervals. Using the input data from each of the SAGE III/ISS  
204 occultations and spherical geometry relations, for every tangent altitude, we compute the zenith



205 angles as well as partial pathlengths corresponding to overlying layers. This generates a  
206 pathlength matrix like the one used in the standard retrieval. Appropriate O<sub>3</sub> twilight ratios are  
207 then obtained by interpolation using the zenith angle and layer altitude. Multiplication of the  
208 standard pathlength matrix by the O<sub>3</sub> ratios yields the modified pathlength matrix including the  
209 effects of diurnal variations.

210

211 The twilight ratios can either be used to modify the O<sub>3</sub> profiles from the standard retrieval or be  
212 incorporated in a new retrieval from measured transmission profile. The first method is like the  
213 procedure described by Dube et al. (2021) for making diurnal corrections to stratospheric NO<sub>2</sub>  
214 data from SAGE III/ISS. The archived SAGE III/ISS O<sub>3</sub> profile and the standard pathlength  
215 matrix are used to recreate the O<sub>3</sub> specific slant optical depth, as shown by the equation

$$216 \quad \tau = \sigma S n, \quad (1)$$

217 where  $\tau$  is the O<sub>3</sub> slant optical depth profile,  $\sigma$  is the O<sub>3</sub> cross section corresponding to the center  
218 wavelength of PG1, and  $n$  is the O<sub>3</sub> profile from the standard retrieval.  $S$  represents the  
219 pathlength matrix with each row corresponding to a tangent point altitude. This can be written as  
220 a triangular matrix because of the geometric symmetry on opposite sides of the tangent point as  
221 can be seen from Figure 2. The slant optical depth can then be converted to a O<sub>3</sub> vertical profile  
222 corrected for diurnal variations using the modified pathlength matrix described earlier, as shown  
223 by the equation

$$224 \quad n_{wd} = (S_{wd})^{-1} \tau / \sigma = (S_{wd})^{-1} S n \quad (2)$$

225 where  $S_{wd}$  is the modified pathlength matrix with diurnal correction and  $n_{wd}$  is the corrected O<sub>3</sub>  
226 profile. Here it is assumed that the O<sub>3</sub> absorption coefficient remains constant along the LOS.

227 This procedure gives a quantitative estimate of the over-prediction by the standard retrieval. The



228 results for a sunrise event on June 14, 2021 (Event ID =2021061438SR) are shown in Figure 6.  
229 The left panel displays the O<sub>3</sub> concentration profiles – the solid red line is the archived data from  
230 standard retrieval and the solid black line represents the profile after applying the diurnal  
231 correction ratios to the pathlength matrix. The percent difference between the standard and the  
232 modified profiles is shown by the solid line on the right panel. For this occultation, the difference  
233 exceeds 40% above 64 km. This is consistent with the change in O<sub>3</sub> slant column due to the  
234 diurnal correction shown in Figure 3. The right panel in Figure 3 shows around 30% increase in  
235 the slant-path column between 61 and 72 km. We also note that the retrieval becomes noisy in  
236 the upper altitudes as O<sub>3</sub> concentrations reach near detection limits. In the second method,  
237 instead of evaluating the slant optical depth using equation 1, the archived slant-path  
238 transmission data, which corresponds to PG1, is used along with the standard and modified  
239 pathlength matrices to retrieve the vertical O<sub>3</sub> profiles. The change in the slant-path transmission  
240 corresponding to the science CCD channel PG 1 for each tangent altitude below an upper  
241 boundary of 90 km is related to the total slant optical depth made up mainly of O<sub>3</sub> absorption and  
242 Rayleigh scattering contributions. After removing the Rayleigh scattering part corresponding to  
243 the center wavelength of 286.124 nm, the slant-path O<sub>3</sub> column can be estimated using the O<sub>3</sub>  
244 absorption coefficient at this wavelength taken from Bogumil et al. (2003), which is the same  
245 database used in the SAGE retrieval algorithm. The standard and modified pathlength matrices  
246 are then used to get the vertical O<sub>3</sub> profiles both without and with corrections for diurnal  
247 variations. The retrieved O<sub>3</sub> profiles for the sunrise event mentioned earlier are given by the  
248 dashed lines on the left panel of Figure 6, the red color denoting the standard retrieval without  
249 diurnal corrections and the black color the modified retrieval with diurnal corrections. We have  
250 used a very simple algorithm and assumed that the transmission data corresponds to a single



251 wavelength to simplify the calculation. The actual retrieval procedure used for the archived  
252 products may have included more refinements. The agreement between results of the two  
253 different methods is very good, both for the vertical O<sub>3</sub> profiles and for the percent differences.  
254 Results for a sunset event, closer to the above sunrise event in location and within a day (Sunset  
255 event ID = 2021061515SS) are shown in Figure 7. The impact of the diurnal correction is much  
256 smaller for sunset conditions. The maximum difference between the standard and modified  
257 profiles is less than 10%. The two different procedures for incorporating diurnal effects yield  
258 very nearly same results.

259

260 We have applied the diurnal corrections following the procedure described above to all the  
261 SAGE III/ISS measurements from June 2021, categorized by the event type of sunrise or sunset.  
262 Individual O<sub>3</sub> profiles were grouped together in 11 latitude bands, 11.25° wide between 56.25°N  
263 and 56.25°S. The percent difference between the standard retrieval profile and the corresponding  
264 modified profile, defined as  $(O_3/O_{3, WD} - 1) * 100$ , was calculated and the mean for each latitude  
265 band was evaluated. Figure 8 shows the resulting distribution of the mean, which represents the  
266 over-estimation by the standard retrieval, as a function of latitude and altitude. There is a  
267 latitudinal dependence with peak values occurring near 64 km and the summer hemisphere  
268 showing smaller difference. Values higher than 100% (dark violet region) are seen in the upper  
269 altitudes of the winter hemisphere. The O<sub>3</sub> profile has a sharp gradient reaching a very low  
270 minimum in winter between and 70 and 80 km. The retrieved data in this region are very noisy  
271 and thus sometimes include negative concentrations. The percent difference between the two  
272 retrievals also displays a very noisy distribution with large values of both signs. Near the upper  
273 boundary of 90 km, the data is smooth, and the bias caused by the diurnal variations is very



274 small. At these high altitudes, the day-night terminator occurs at higher solar zenith angles and  
275 the variation around  $90^\circ$  is small. The distribution of percent differences for sunset  
276 measurements is shown in Figure 9. The values are much smaller as discussed earlier, since the  
277 diurnal corrections are not significant for sunset. To look at the seasonal dependence of the  
278 impact of diurnal corrections on the retrieved  $O_3$ , we have repeated the procedure with SAGE  
279 III/ISS data from January 2021. Figure 10 displays the results for sunrise conditions. The  
280 differences between the standard and modified retrievals are larger again in the winter  
281 hemisphere with peak values occurring near 64 km. This agrees qualitatively with Figure 11 of  
282 Natarajan et al. (2005), which showed the percent difference in retrieved HALOE sunrise  $O_3$  for  
283 January 1995 with updated diurnal correction factors compared to the retrieval with HALOE  
284 version 19 correction factors. The archived HALOE version 19 retrieval used correction factors  
285 from a diurnal calculation at 61 km for all mesospheric tangent altitudes above. Since a partially  
286 corrected (version 19) retrieval was used as the basis, the contour levels are negative and smaller  
287 in magnitude.

288

#### 289 **4 Sunrise to Sunset Ratio**

290

291 Brühl et al. (1996), in their paper on HALOE  $O_3$  channel validation, discussed the sunrise to  
292 sunset differences in  $O_3$  around 0.1 hPa (about 64 km). Mesospheric layers are under sunlit  
293 conditions even at zenith angles slightly greater than  $90^\circ$  at dawn and dusk. As explained earlier,  
294 the viewing geometry in solar occultation observations leads to an increase in the  $O_3$  optical  
295 depth because  $O_3$  concentrations corresponding to varying zenith angles greater than  $90^\circ$  are seen  
296 along the LOS. We have noted that the impact is larger during sunrise than sunset measurement.



297 The sunrise to sunset O<sub>3</sub> concentration ratio becomes larger if the diurnal variations along the  
298 LOS are not considered in the retrieval. Solar occultation experiments occasionally offer the  
299 opportunity to approximately check this ratio as a test of consistency of measurement and  
300 agreement with theory. This is possible when sunrise and sunset orbits cross over each other  
301 within a reasonably short interval of time and physical proximity. Such near coincidences are  
302 quite rare. We selected sunrise/sunset pairs of measurements by SAGE III/ISS having tangent  
303 locations within 1.5° latitude, and 15° longitude of each other and separated by a maximum of 36  
304 hours. The effect of advection by the prevailing westerly wind requires that the time and  
305 longitude differences are in the correct direction. There are just 10 pairs of sunrise /sunset  
306 measurements in June 2021 that satisfy the above criteria, all of them in low latitudes with a  
307 mean latitude of 10.46°S at sunrise and 10.27°S at sunset. The mean of the sunrise to sunset ratio  
308 of O<sub>3</sub> concentration for these 10 scans is shown in Figure 11. The solid line corresponding to the  
309 standard retrieval shows ratios greater than 1.1 in the altitude range considered. The modified  
310 retrieval yields a ratio shown by the dashed line decreasing from 1.01 at 60 km to lower values  
311 above. The diamond symbols represent the ratio from the diurnal model and the decreasing  
312 model value with altitude is in qualitative agreement with the modified retrieval. This  
313 comparison serves as an independent criterion to highlight the importance of including the LOS  
314 variations in the retrieval of mesospheric O<sub>3</sub> in solar occultation measurements. We noticed that  
315 very few such pairs of measurements occurred during other months in SAGE III/ISS data, which  
316 satisfied the criteria we have chosen. We have also looked at the latitudinally averaged sunrise  
317 and sunset data for June 2021 obtained for generating figures 8 and 9. For the latitude band  
318 centered at 11.25° S, the sunrise to sunset ratio as a function altitude (not shown) is similar to



319 Figure 11, which used only collocated data. Other independent measurements are needed to  
320 verify the altitude variation of the ratio of sunrise to sunset O<sub>3</sub> concentrations.

321

## 322 **5 Summary**

323

324 Photochemically induced changes in species concentration at twilight can cause asymmetries in  
325 the distribution along the LOS of a solar occultation observation, variations that must be  
326 considered in the retrieval algorithm. Prominent among the species that need corrections for  
327 twilight variations are NO and NO<sub>2</sub> in the stratosphere and O<sub>3</sub> in the mesosphere. The SAGE  
328 III/ISS instrument uses the measurements in the short-wave Hartley-Huggins band to get  
329 mesospheric O<sub>3</sub> profiles. The standard retrieval procedure does not consider the LOS variations  
330 in O<sub>3</sub> caused by photochemistry. This study describes a procedure to use results from diurnal  
331 photochemical model simulations to develop correction factors for different altitudes, latitudes,  
332 and months. These factors were used along with the archived SAGE III/ISS mesospheric O<sub>3</sub> data  
333 for selected time periods to obtain modified O<sub>3</sub> profiles. For the month of June 2021, it is shown  
334 that neglecting the diurnal variations can result in over 30% overestimation of O<sub>3</sub> at 64 km and  
335 low latitudes. An approximate retrieval using the transmission data from SAGE III/ISS also  
336 indicates similar behavior in the profiles obtained with and without diurnal corrections. The  
337 retrievals were repeated for January 2021 to study the seasonal impact. Larger differences are  
338 seen generally between 70 and 80 km in high latitude winter hemisphere, and this is most likely  
339 due to very low O<sub>3</sub> concentrations and large uncertainties in the data. The results from this study  
340 are in good agreement with those obtained for the retrieval of HALOE mesospheric O<sub>3</sub> data.

341



342 SAGE III/ISS data include a few nearly collocated sunrise and sunset measurements, mostly in  
343 the low latitudes and about a day apart. There are 10 pairs of such sunrise and sunset  
344 measurements in June 2021. An analysis of the sunrise to sunset ratio profile from these data  
345 indicates that the retrievals that include the diurnal variations show qualitatively better agreement  
346 with theoretical prediction. We note that dynamical causes such as diurnal tides may also  
347 introduce variations in the sunrise to sunset O<sub>3</sub> ratio especially in the low latitudes. The diurnal  
348 corrections described for occultation retrievals depend mainly on the short period variations  
349 around 90° solar zenith angle and dynamical impacts will not be significant compared to the  
350 photochemical effects.

351

#### 352 **Data Availability**

353 SAGE III/ISS version 5.2 data is available from [https://asdc.larc.nasa.gov/project/SAGE%20III-](https://asdc.larc.nasa.gov/project/SAGE%20III-ISS/g3bssp_52)  
354 [ISS/g3bssp\\_52](https://asdc.larc.nasa.gov/project/SAGE%20III-ISS/g3bssp_52). The O<sub>3</sub> twilight ratios used in this study are available from the author. They can  
355 also be obtained from any diurnal photochemical model of the mesosphere.

356

#### 357 **Author Contribution**

358 MN conducted the photochemical model calculations, SAGE III/ISS O<sub>3</sub> retrievals, and the  
359 analyses described in the study, and he wrote the manuscript. RD and DF provided information  
360 and guidance on the use of SAGE III/ISS mesospheric O<sub>3</sub> data as well as comments on the  
361 manuscript.

362

#### 363 **Competing Interests**

364 The authors declare that there is no competing interest for this study.



365

366 **Acknowledgements**

367 SAGE III/ISS data used in this study were obtained from the NASA Langley Research Center  
368 Atmospheric Science Data Center. MN carried out this work while serving as a Distinguished  
369 Research Associate of the Science Directorate at NASA Langley Research Center.

370

371 **References**

372 Bogumil, K., Orphal, J., Homann, S., Voigt, P., Spietz, O., Fleischmann, A., Vogel, M.,  
373 Hartmann, H., Bovensmann, J., Frerick, J., and Burrows, J.: Measurements of molecular  
374 absorption spectra with the SCIAMACHY pre-flight model: instrument characterization and  
375 reference data for atmospheric remote sensing in the 230-2380 nm region, *J. Photochemistry and*  
376 *Photobiology A: Chemistry*, Vol 157, No. 2-3, 167-184, 2003.

377 Boughner R. E., Larsen, J. E., and Natarajan., M.: The influence of NO and ClO variations at  
378 twilight on the interpretation of solar occultation measurements, *Geophys. Res. Lett.*, 7, 231 –  
379 234, 1980.

380 Brohede, S. M., Haley, C. S., McLinden, C. A., Sioris, C. E., Murtagh, D. P., Petelina, S. V.,  
381 Llewellyn, E. J., Bazureau, A., Goutail, F., Randall, C. E., Lumpe, J. D., Taha, G., Thomasson,  
382 L. W., and Gordley, L. L.: Validation of Odin/OSIRIS stratospheric NO<sub>2</sub> profiles, *J. Geophys.*  
383 *Res.-Atmos.*, 112, D07310, <https://doi.org/10.1029/2006JD007586>, 2007.

384 Brühl, C., Drayson, S. R., Russell III, J. M., Crutzen, P. J., McInerney, J. M., Purcell, P. N.,  
385 Claude, H., Gernandt, H., McGee, T. J., McDermid, I. S., and Gunson, M. R.: Halogen  
386 Occultation Experiment ozone channel validation, *J. Geophys. Res.*, Vol. 101, NO. D6, 10,217 -  
387 10,240, 1996.



- 388 Dube, K., Bourassa, A., Zawada, D., Degenstein, D., Damadeo, R., Flittner, D., and Randel, W.:
- 389 Accounting for the photochemical variation in stratospheric NO<sub>2</sub> in the SAGE III/ISS solar
- 390 occultation retrieval, *Atmos. Meas. Tech.*, 14, 557 – 566, [https://doi.org/10.5194/amt-14-557-](https://doi.org/10.5194/amt-14-557-2021)
- 391 [2021](https://doi.org/10.5194/amt-14-557-2021), 2021.
- 392 Gordley, L. L., Russell III, J. M., Mickley, L. J., Frederick, J. E., Park, J. H., Stone, K. A.,
- 393 Beaver, G. M., McInerney, J. M., Deaver, L. E., Toon, G. C., Murcray, F. J., Blatherwick, R. D.,
- 394 Gunson, M. R., Abbatt, J. P. D., Mauldin III, R. L., Mount, G. H., Sen, B., and Blavier, J. F.:
- 395 Validation of nitric oxide and nitrogen dioxide measurements made by the Halogen Occultation
- 396 Experiment for UARS platform, *J. Geophys. Res.-Atmos.*, 101, 10241–10266, 1996.
- 397 JPL Publication 19-5, Chemical Kinetics and Photochemical Data for Use in Atmospheric
- 398 Studies, Evaluation Number 19, 2020. [https://jpldataeval.jpl.nasa.gov/pdf/NASA-](https://jpldataeval.jpl.nasa.gov/pdf/NASA-JPL%20Evaluation%2019-5.pdf)
- 399 [JPL%20Evaluation%2019-5.pdf](https://jpldataeval.jpl.nasa.gov/pdf/NASA-JPL%20Evaluation%2019-5.pdf)
- 400 McCormick, M. P., Lei, L., Hill, M. T., Anderson, J., Querel, R., and Steinbrecht, W.: Early
- 401 results and validation of SAGE III-ISS ozone profile measurements from onboard the
- 402 International Space Station, *Atmos. Meas. Tech.*, 13, 1287-1297, [https://doi.org/10.5194/amt-13-](https://doi.org/10.5194/amt-13-1287-2020)
- 403 [1287-2020](https://doi.org/10.5194/amt-13-1287-2020), 2020.
- 404 Natarajan, M., Deaver, L. E., Thompson, E., and Magill, B.: Impact of twilight gradients on the
- 405 retrieval of mesospheric ozone from HALOE, *J. Geophys. Res.*, Vol. 110,
- 406 doi:10.1029/2004JD005719, 2005.
- 407 Newchurch, M. J., Allen, M., Gunson, M. R., Salawitch, R. J., Collins, G. B., Huston, K. H.,
- 408 Abbas, M. M., Abrams, M. C., Chang, A. Y., Fahey, D. W., Gao, R. S., Irion, F. W.,
- 409 Loewenstein, M., Manney, G. L., Michelson, H. A., Podolske, J. R., Rinsland, C. P., and Zander,



410 R.: Stratospheric NO and NO<sub>2</sub> abundances from ATMOS Solar-Occultation Measurements,  
411 Geophys. Res. Lett., 23, 2373-2376., <https://doi.org/10.1029/96GL01196.1996>.

412 Russell III, J. M., Farmer, C. B., Rinsland, C. P., Zander, R., Froidevaux, L., Toon, G. C., Gai,  
413 B., Shaw, J., and Gunson, M.: Measurements of Odd Nitrogen Compounds in the Stratosphere  
414 by the ATMOS Experiment on Spacelab 3, J. Geophys. Res., Vol 3, D2, 1718-1736, 1988.

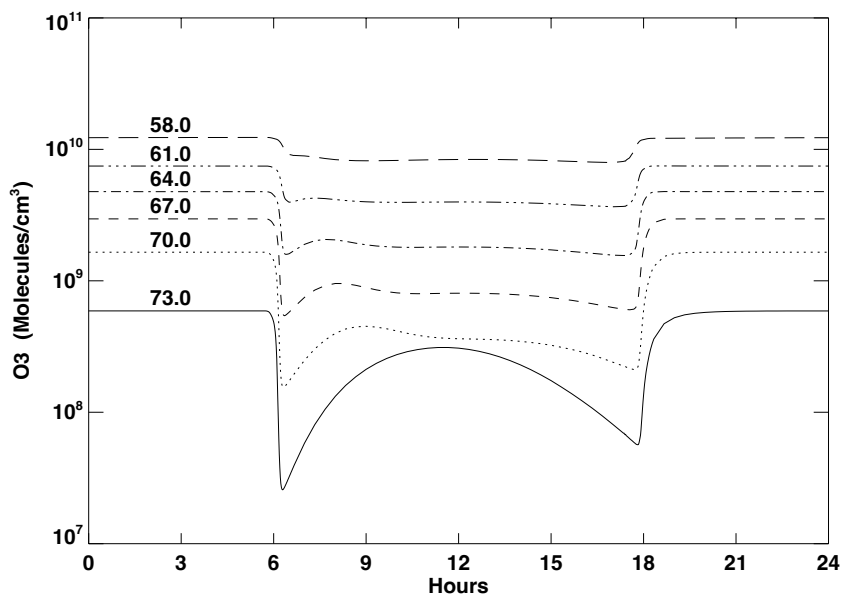
415 SAGE III Algorithm Theoretical Basis Document (ATBD) Solar and Lunar Algorithm, LaRC  
416 475-00-109, Version 2.1, 2002. [https://eosps0.gsfc.nasa.gov/sites/default/files/atbd/atbd-sage-](https://eosps0.gsfc.nasa.gov/sites/default/files/atbd/atbd-sage-solar-lunar.pdf)  
417 [solar-lunar.pdf](https://eosps0.gsfc.nasa.gov/sites/default/files/atbd/atbd-sage-solar-lunar.pdf)

418 SAGE III/ISS Data Products User's Guide, Version 3.0, 2021.  
419 <https://asdc.larc.nasa.gov/documents/sageiii-iss/guide/DPUG-G3B-2-0.pdf>

420 Wang, H. J. R., Damadeo, R., Flittner, D., Kramarova, N., Taha, G., Davis, S., et al.: Validation  
421 of SAGE III/ISS solar occultation ozone products with correlative satellite and ground-based  
422 measurements, J. Geophys. Res., 125, e2020JD032430. <https://doi.org/10.1029/2020JD032430>  
423



424



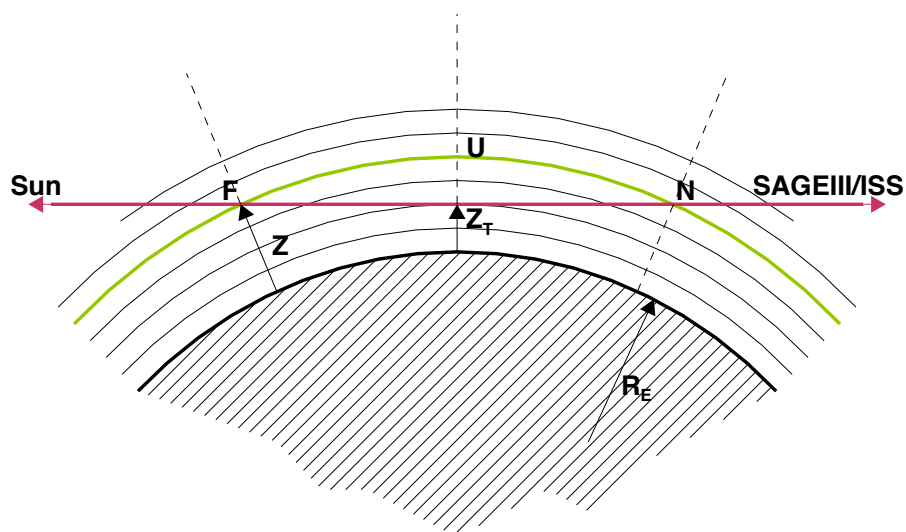
425

426

427

428 Figure 1. Diurnal variation in O<sub>3</sub> at 11.25°S in June at altitudes from 58 to 73 km. 0 hours

429 denote midnight.

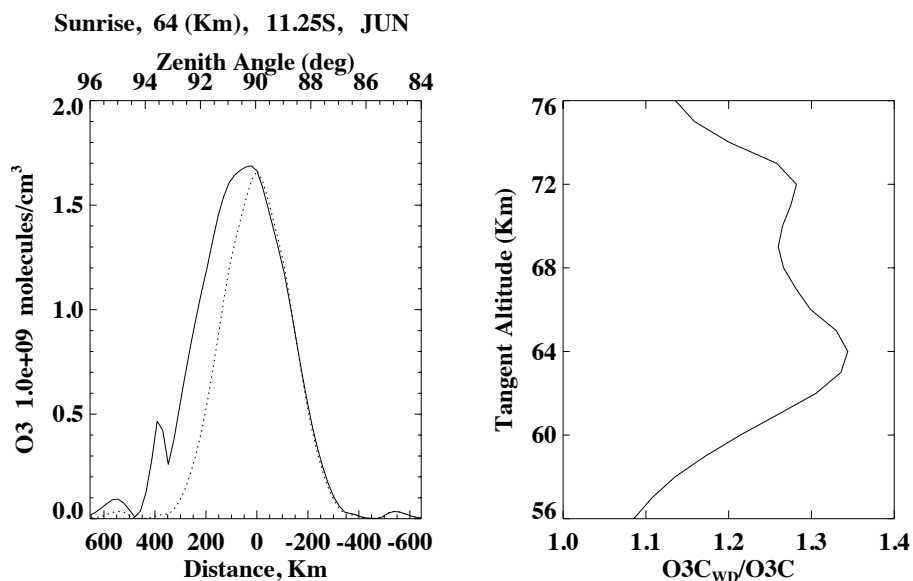


430

431 Figure 2. Schematic representation of the solar occultation measurement.  $Z_T$  is the tangent  
432 altitude, red line is the LOS,  $Z$  is the altitude of a layer above the tangent altitude,  $F$  (towards  
433 sun) and  $N$  (towards SAGE III/ISS) are the points of intersection of layer at  $Z$  with the LOS, and  
434  $R_E$  is the earth radius.

435

436



437

438

439

440 Figure 3. (Left) O<sub>3</sub> concentration along the LOS for a tangent altitude of 64 km at 11.25°S

441 latitude in June. Solid line shows O<sub>3</sub> with diurnal variations and the dotted line represents O<sub>3</sub>

442 without diurnal variations. (Right) Ratio of the O<sub>3</sub> column along the LOS with appropriate

443 diurnal variations to the O<sub>3</sub> column without diurnal variations, plotted as a function of altitude at

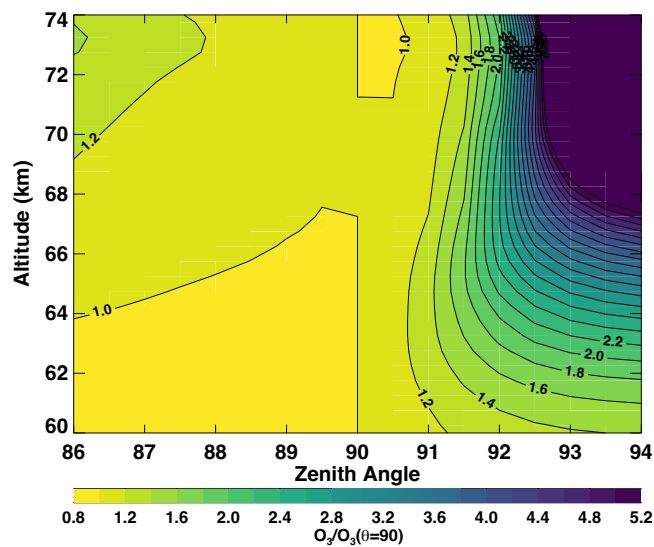
444 11.25°S in June.

445

446



447



448

449

450

451 Figure 4. Ozone twilight ratio, defined as  $O_3$  at zenith angle  $\theta/O_3$  at  $\theta=90^\circ$ , as a function of

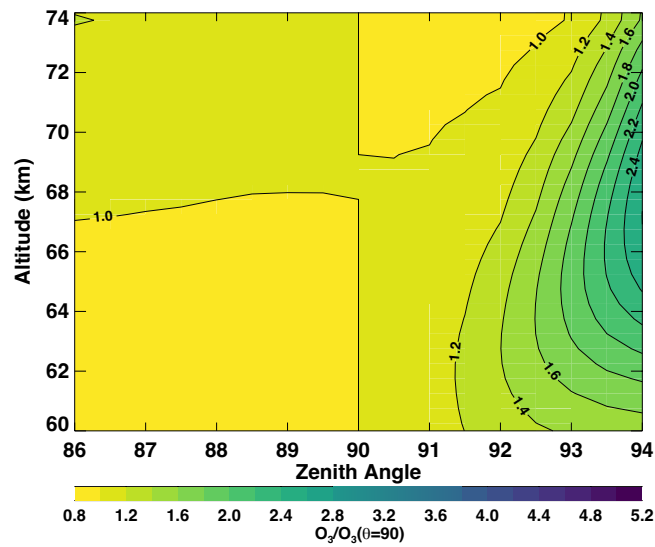
452 zenith angle and altitude for sunrise in June and  $11.25^\circ$  latitude.

453

454

455

456



457

458

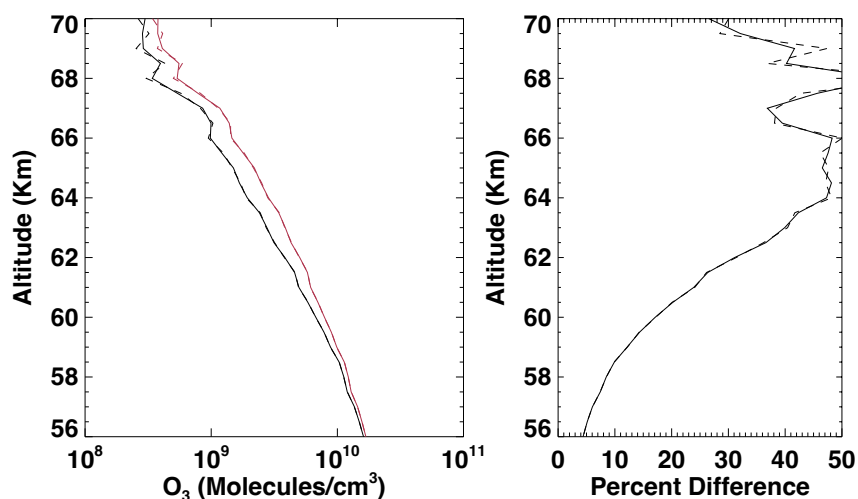
459

460 Figure 5. Same as Figure 4 for sunset conditions

461

462

463



464

465

466 Figure 6. SAGE III/ISS sunrise O<sub>3</sub> for a sunrise event on June 14, 2021 (Event ID 2021061438SR).

467 (Left panel) Red solid line shows the standard SAGE III retrieval, and the black solid line

468 represents the retrieval including the diurnal variations along LOS. The dashed lines represent

469 the retrievals using the transmission data, the red color for the standard retrieval and the black

470 denoting the retrieval with diurnal corrections. (Right panel) Percent difference between the

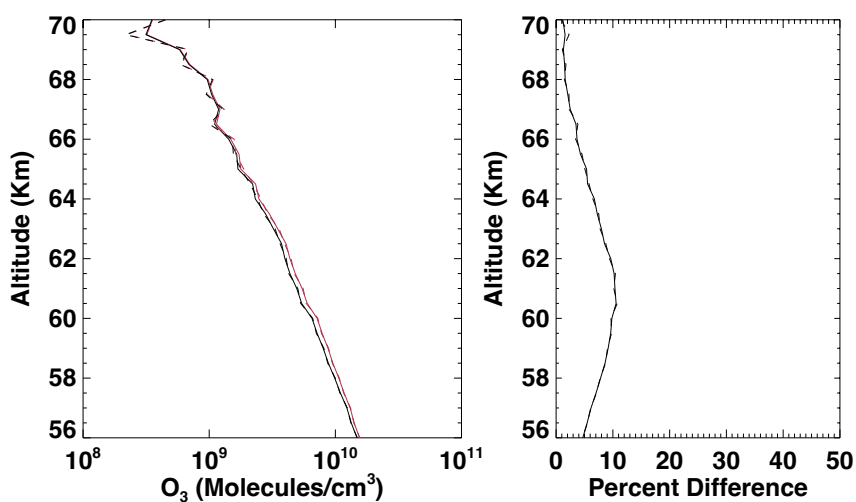
471 standard retrieval and the one with diurnal corrections; solid line using the archived standard

472 retrieval of O<sub>3</sub> concentration, and the dashed line based on the approximate retrieval using the

473 transmission data.



474



475

476

477 Figure 7. Same as Figure 6 but for a sunset event (Event ID 2021061515SS) closer to the sunrise  
478 event shown in Figure 6.

479

480

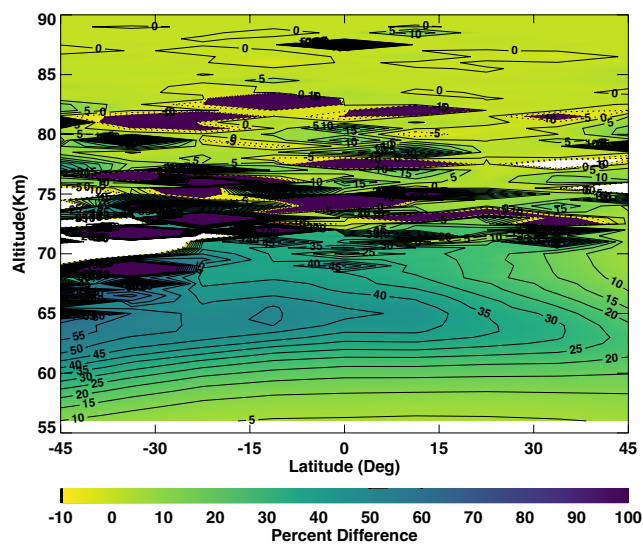
481

482



483

484



485

486

487

488 Figure 8. Latitudinal average of the percent difference in sunrise O<sub>3</sub> between the standard  
489 (archived) retrieval and a retrieval including diurnal variations along the LOS, as a function of  
490 latitude and altitude for June 2021

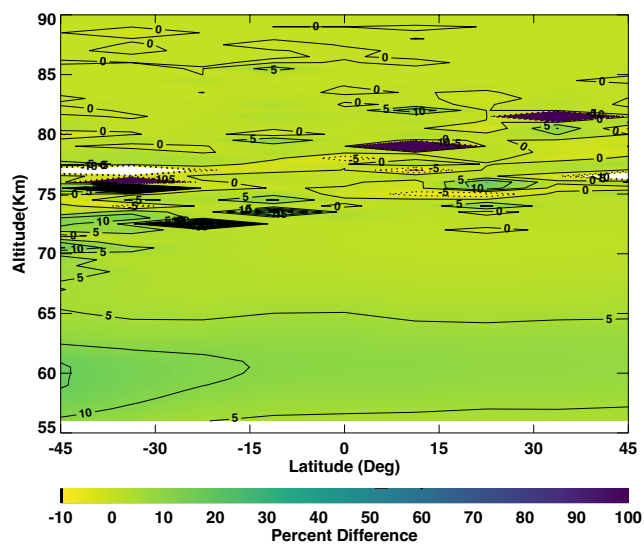
491

492



493

494

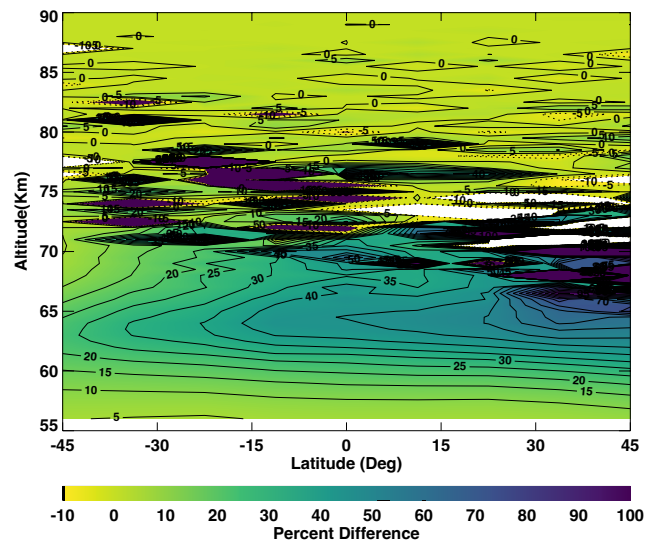


495

496

497

498 Figure 9. Same as Figure 8 but for sunset conditions.



499

500

501

502 Figure 10. Same as Figure 8 but for January 2021.

503

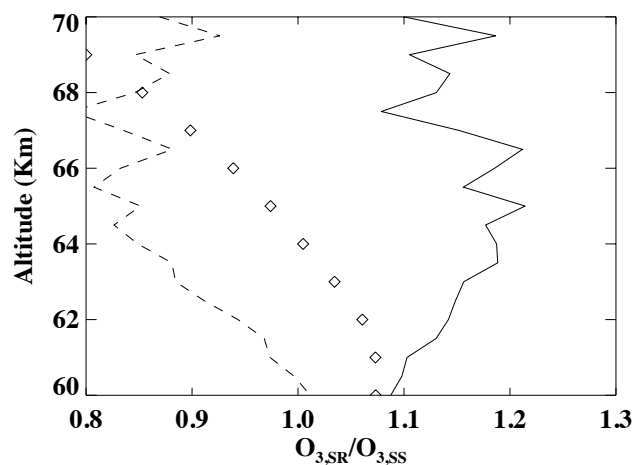
504

505

506

507

508



509

510

511 Figure 11. Vertical profile of  $O_3$  sunrise to sunset ratio in June 2021. Nearly collocated 10 pairs  
512 of sunrises (mean latitude  $10.46^\circ\text{S}$ ) and sunsets (mean latitude  $10.27^\circ\text{S}$ ) data are used for this  
513 plot. Solid line represents the standard (archived) retrieval, and the dashed line shows the  
514 retrieval including diurnal variations along the LOS. The diamond symbols are from diurnal  
515 photochemical calculations at  $11.25^\circ\text{S}$  for June.